

# Orientational correlation and velocity distributions in uniform shear flow of a dilute granular gas

Bishakdatta Gayen<sup>1</sup> and Meheboob Alam<sup>1,2\*</sup>

<sup>1</sup>*Engineering Mechanics Unit,* <sup>2</sup>*Max Planck Partner Group of MPI-Bremen,*

*Jawaharlal Nehru Center for Advanced Scientific Research, Jakkur PO, Bangalore 560064, India*

(Dated: October 23, 2018)

Using particle simulations of the uniform shear flow of a rough dilute granular gas, we show that the translational and rotational velocities are strongly correlated in direction, but there is no orientational correlation-induced singularity at perfectly smooth ( $\beta = -1$ ) and rough ( $\beta = 1$ ) limits for elastic collisions ( $e = 1$ ); both the translational and rotational velocity distribution functions remain close to a Gaussian for these two limiting cases. Away from these two limits, the orientational as well as spatial velocity correlations are responsible for the emergence of non-Gaussian high velocity tails. The tails of both distribution functions follow stretched exponentials, with the exponents depending on normal ( $e$ ) and tangential ( $\beta$ ) restitution coefficients.

PACS numbers: 45.70.Mg, 47.45.-n, 45.70.-n

Under external forcing (e.g. shearing/vibration), the granular materials, a collection of macroscopic solid particles, can flow like a gas or a liquid. The rapid flow of granular gases (dilute limit) has been extensively studied using kinetic theory [1, 2, 3] that takes into account the dissipative nature of particle interactions. Most theories of granular gases assume that the particles are *smooth* which is a simplification of real particles which are always *rough*, giving rise to surface friction, and the rotational motion is important to deal with such rough, frictional particles. Prior literature [2, 3, 4, 5, 6] suggests that the rotational motion should not be neglected for a realistic modeling of the dynamics and pattern formation in a granular gas even in the Boltzmann (dilute) limit. For example, the molecular dynamics (MD) simulations[6] have elucidated the crucial role of friction on pattern formation in oscillated granular layers via a comparison with experimental

---

\* Author to whom correspondence should be addressed: meheboob@jncasr.ac.in;

To be published in *Physical Review Letters*, vol. 100, (2008)

results. Despite the importance of frictional interactions, only a small-body of work exists on the modeling of rough granular gas [2, 3, 4, 5].

To develop constitutive models of rough granular gases, a systematic study of correlations and the distribution functions of both ‘translational’ and ‘rotational’ velocities is of fundamental interest. While the deviation of translational velocity distribution functions (VDF) from a Gaussian has been extensively studied (in terms of stretched exponential or power-law tails) using theory [7], simulation [8] and experiment [9], similar results on ‘rotational’ VDFs are very scarce.

For a ‘rough’ granular gas, one needs to probe possible ‘orientational’/‘directional’ correlations between translation and rotation, in addition to standard density and velocity correlations. It has been recently found [5] that such orientational correlations are strong and the limit of smooth granular gas is *singular* in a freely cooling granular gas. The last result readily raises doubts about the validity of the hydrodynamic theories [4] that are obtained via perturbative expansions around the smooth-particle limit. Also, it is of interest to ascertain the impact of such orientational correlation on VDFs, especially in two limits of perfectly smooth and rough particles around which the perturbative expansions are sought. The above issues are investigated in this paper using MD simulations of the *uniform shear* flow (which is a prototype non-equilibrium steady-state to develop constitutive relations[4]) of a dilute rough granular gas.

We consider a mono-disperse system of *rough*, inelastic spheres of diameter  $d$ , mass  $m$ , and the moment of inertia  $\mathcal{I}$ , interacting via purely repulsive potential. Let us denote the *pre-collisional* translational and rotational velocities of particle  $i$  by  $\mathbf{c}_i$  and  $\boldsymbol{\omega}_i$ , respectively, and the corresponding *post-collisional* velocities are denoted by the primed symbols,  $\mathbf{c}'_i$  and  $\boldsymbol{\omega}'_i$ . The pre-collisional relative velocity at contact,  $\mathbf{g}_{ij}$ , between particle  $i$  and  $j$  is  $\mathbf{g}_{ij} = \mathbf{c}_{ij} - (d/2)\mathbf{k} \times (\boldsymbol{\omega}_i + \boldsymbol{\omega}_j)$ , where  $\mathbf{c}_{ij} = \mathbf{c}_i - \mathbf{c}_j$  is the relative translational velocity between particle  $i$  and  $j$ , and  $\mathbf{k}$  is the unit vector directed from the center of particle  $j$  to that of particle  $i$ . Neglecting Coulomb friction in the dilute limit, we have the following collision model[2]:

$$\mathbf{k} \cdot \mathbf{g}'_{ij} = -e(\mathbf{k} \cdot \mathbf{g}_{ij}) \quad \text{and} \quad \mathbf{k} \times \mathbf{g}'_{ij} = -\beta(\mathbf{k} \times \mathbf{g}_{ij}),$$

characterized by two parameters: the normal restitution coefficient,  $0 \leq e \leq 1$ , and the tangential restitution coefficient,  $-1 \leq \beta \leq 1$ . The former is an indicator of the *inelasticity* of particle-collisions and the latter characterizes its surface roughness. For collisions between perfectly smooth particles  $\beta = -1$ , with increasing value of  $\beta$  being an indicator of the increasing degrees of particle surface friction. The value of  $\beta = 0$  represent the case for which the particle

surface friction and inelasticity are sufficient to eliminate the post-collisional tangential relative velocities. For  $0 < \beta \leq 1$ , the *spin-reversal* occurs after collision[2], and the case of  $\beta = 1$  corresponds to collisions between perfectly rough particles.

We have used an event-driven algorithm [10] to simulate the uniform shear flow, characterized by a linear velocity profile. The simulation box is a cube, with Lees-Edwards boundary condition [11] across two moving boundaries along  $y$ -direction, and the periodic boundary conditions along  $x$ - and  $z$ -directions, with  $x$  being the direction of flow. The positions of particles are initialized in the simulation box, with their translational and rotational velocities being chosen randomly from a Gaussian distribution. The data are accumulated once the system has reached a statistical steady-state condition which is monitored from the temporal evolution of the system's kinetic energy. The coarse-grained 'translational' fluctuation kinetic energy (i.e. the standard granular temperature),  $T$ , and the 'rotational' fluctuation kinetic energy,  $\theta$ , are defined as:  $T(\mathbf{x}, t) = \langle \mathbf{C} \cdot \mathbf{C} \rangle / 3$  and  $\theta(\mathbf{x}, t) = (\mathcal{I}/3m) \langle \Omega \cdot \Omega \rangle$ , respectively, where the angular bracket denotes a suitable averaging. Here  $\mathbf{C} = \mathbf{c} - \langle \mathbf{c} \rangle$  is the translational 'peculiar' velocity which measures the deviation of the instantaneous particle velocity from the local mean velocity ( $\langle \mathbf{c} \rangle$ ), and  $\Omega = \boldsymbol{\omega} - \langle \boldsymbol{\omega} \rangle$  is its rotational counterpart. All results are presented for a very dilute system (Boltzmann limit), with a volume fraction of  $\phi = 0.01$ . (The effect of density, as well as Coulomb friction, is a non-trivial issue which will be taken up in a separate publication.) The number of particles was fixed to  $N = 8000$ , and the robustness of results was checked by using  $N = 4000$  and  $16000$ .

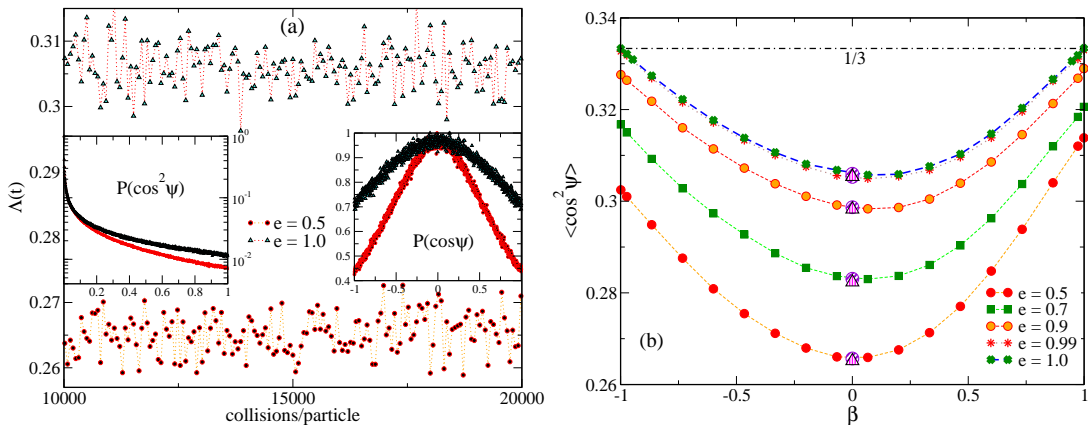


FIG. 1: (color online) (a) Variation of  $\Lambda(t) = \cos^2 \Psi$  with time for different values of  $e$  with  $\beta = 0$ ,  $\phi = 0.01$  and  $N = 8000$ . Left and right insets show the distributions of  $\cos^2 \Psi$  and  $\cos \Psi$ , respectively. (b) Variation of  $\langle \cos^2 \Psi \rangle$  with  $\beta$  for different  $e$ . Larger symbols (triangle and hatched-circle) at  $\beta = 0$  for each  $e$  correspond to simulations with  $N = 4000$  and  $16000$ , respectively.

It is known that the translational and rotational fluctuating velocities are uncorrelated in a molecular gas, but they have been shown to be correlated (in direction) in a freely cooling granular gas [5]. This orientational/directional correlation between translational and rotational velocities is quantified in terms of the mean square of the cosine of the angle,  $\Psi$ , between  $C = \mathbf{c} - \langle \mathbf{c} \rangle$  and  $\Omega = \boldsymbol{\omega} - \langle \boldsymbol{\omega} \rangle$ :

$$\Lambda(t) = \frac{1}{N} \sum_{i=1}^N \frac{(C_i \cdot \Omega_i)^2}{(C_i^2 \Omega_i^2)} = \frac{1}{N} \sum_{i=1}^N \cos^2 \Psi_i \equiv \cos^2 \Psi. \quad (1)$$

In fig. 1(a) we have plotted the temporal variation of  $\Lambda(t)$  (main panel) for two values of normal restitution coefficients ( $e = 1, 0.5$ ), with the tangential restitution coefficient being set to  $\beta = 0$ ; the corresponding probability distribution of  $\cos^2 \Psi$  is shown in the left inset. (The probability distribution of  $\cos \Psi$ ,  $P(\cos \Psi)$ , is symmetric about its zero mean for all  $e$ , but its width becomes narrower with decreasing  $e$ , see the right inset.) From the main panel and the left inset, we find that even for  $e = 1$  the mean value of  $\Lambda$  is different from  $1/3$  (for a molecular gas), signaling the presence of *orientational/directional* correlation; decreasing the value of  $e$  to 0.5 decreases its value to  $\langle \Lambda \rangle \sim 0.26$ , thus enhancing orientational correlation significantly. The variation of the temporal-average of  $\Lambda(t)$  with particle roughness,  $\beta$ , is shown in fig. 1(b); the dot-dash line represents the limiting value of  $1/3$  for a molecular gas. Note that the data points for  $e = 1$  (thick blue dashed line) and  $e = 0.99$  almost overlap with each other. For any  $e$ , the orientational correlation is maximum at  $\beta \sim 0$  and it decreases *monotonically* as we approach the perfectly smooth ( $\beta = -1$ ) and perfectly rough ( $\beta = 1$ ) limits. This latter observation is in contrast to that in a freely cooling dilute granular gas [5] for which  $\langle \Lambda \rangle$  varies non-monotonically with  $\beta$  for  $-1 < \beta < 0$  and  $0 < \beta < 1$ . Another difference with freely cooling gas is that the magnitude of  $\langle \Lambda \rangle$  is much larger in shear flow. It must be noted that even though the translation and rotation are decoupled at  $\beta = -1$  (independent of the value of  $e$ ), the smooth limit is singular for any  $e \neq 1$  in shear flow. However, there is no orientational correlation-induced singularity at both the perfectly smooth ( $\beta = -1$ ) and rough ( $\beta = 1$ ) limits for the limiting case of  $e = 1$ .

Before presenting results on VDFs, we probe mean-field quantities to ascertain the presence of any inhomogeneity in our system. Figure 2 shows the probability distributions of the mean density (main panel) and the rotational temperature (right upper inset) for  $\phi = 0.01$  and  $\beta = 0$ ; the distribution of mean translational temperature ( $T$ ) looks similar to that of  $\theta$  (not shown). The lower right inset shows that the translational and rotational temperatures are un-equally partitioned over the whole range of  $\beta$  (except at  $\beta = 1$  with  $e = 1$ ), and the calculated temperature ratio (symbols)

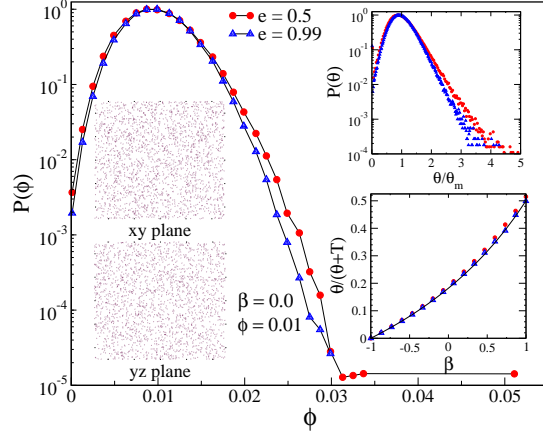


FIG. 2: (color online) Probability distributions of mean density (main panel) and rotational temperature (right upper inset) for different values of  $e$ . Right lower inset shows the variation of temperature ratio,  $\theta/(\theta + T)$ , with  $\beta$ . Two left insets show projected particle snapshots in the  $xy$ - and  $yz$ -planes at steady states for  $e = 0.5$ .

agrees well with theoretical predictions [2, 3] (solid line). The data for mean distributions in Fig. 2 have been obtained by dividing the simulation box into a number of equal-sized cells ( $10^3$ ) such that on average about ten particles occupy each cell and then calculating the instantaneous value of any mean field quantity ( $\phi$ ,  $T$ ,  $\theta$ ,  $\langle \mathbf{c} \rangle$ ) in each cell. It is interesting that even though the mean density varies between 0.003 and 0.017 in about 90% cells, the density-distribution remains almost identical with decreasing  $e$  from 0.99 to 0.5. The projected snapshots of all particles (at steady state after 60000 collisions per particle) in the  $xy$ - and  $yz$ -planes, as displayed in two left insets of Fig. 2, further suggest that the particles are homogeneously distributed and there is no discernible dissipation-induced clustering even at  $e = 0.5$  in our system.

Now we turn to velocity distribution functions which are known to be strongly affected by the presence of correlations [7, 8, 9]. To calculate VDFs, we used *cell-wise* averaging as discussed above. Figure 3(a) shows the probability distribution functions of the translational (main panel) and rotational (lower inset) fluctuating velocities for  $\beta = -0.999$ , while Fig. 3(b) shows the translational (lower inset) and rotational (main panel) VDFs for  $\beta = 0$ . In each plot, two data sets for  $e = 0.99$  and 0.5 have been superimposed, and the black dashed line represents a Gaussian. The horizontal axis of each plot has been scaled by  $\sigma$ , the standard deviation of the corresponding distribution, and the vertical axis scaled such that  $P(0) = 1$ . For the perfectly smooth limit ( $\beta \sim -1$ ) in Fig. 3(a), the tails of the translational VDFs deviate from a Gaussian with increasing dissipa-

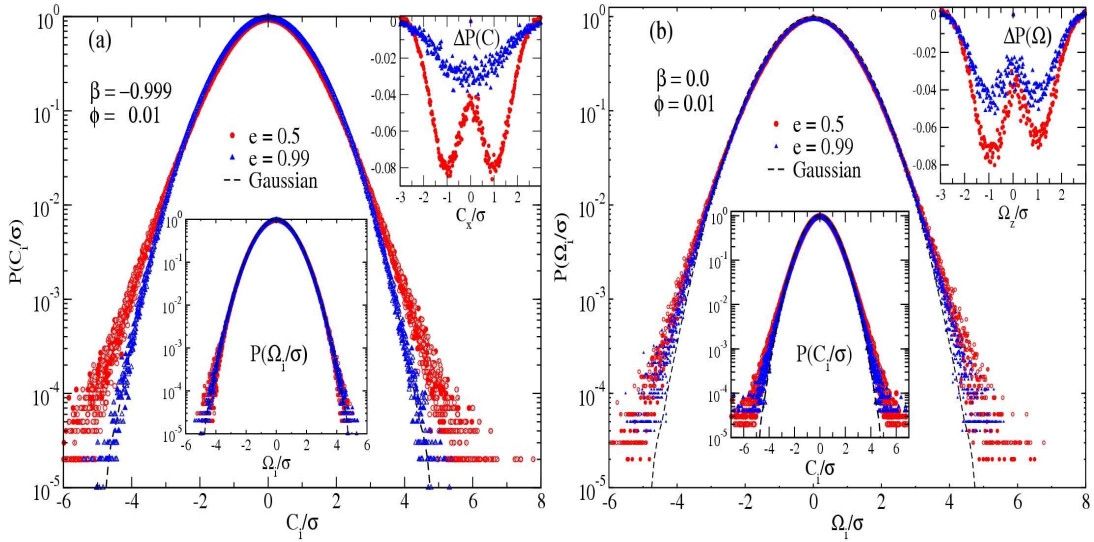


FIG. 3: (color online) (a) Translational (main panel) and rotational (lower inset) VDFs for  $\beta = -0.999$ . (b) Rotational (main panel) and translational (lower inset) VDFs for  $\beta = 0$ . The upper right inset in each panel shows the deviation of the low velocity regions from a Gaussian.

tion; the rotational VDFs remain a Gaussian even for  $e = 0.5$ . We did not find any discernible difference among the VDFs for all three components of each velocity ( $C_i$  and  $\Omega_i$ , with  $i = x, y, z$ ) and that they follow the same distribution for a given  $e$ . For the other extreme of perfectly rough limit ( $\beta \sim 1$ , not shown), the translational VDFs follow a similar behavior as that for  $\beta \sim -1$ , but the rotational VDFs become non-Gaussian with increasing dissipation. At intermediate values of roughness ( $\beta = 0$ ) as in Fig. 3(b), both the translational and rotational velocity distributions deviate from a Gaussian even in the quasi-elastic limit ( $e \sim 1$ ). It is seen that both  $P(C_x)$  and  $P(\Omega_z)$  are under-populated for low-velocities and over-populated for high-velocity tails. The upper right insets in Figs. 3(a) and 3(b) show the deviation of low velocities from a Gaussian (i.e.  $\Delta P(x) = P(x) - \exp(-x^2/2)$ , with  $x = C/\sigma, \Omega/\sigma$ ). It is noteworthy that the low-velocity region of  $P(\Omega_z)$  is slightly asymmetric for  $e = 0.5$ ; such asymmetry is absent for  $\Omega_x$  and  $\Omega_y$  and at higher values of  $e > 0.7$ . Such asymmetry implies the onset of preferential transport of rotational velocity fluctuation along the negative  $z$ -direction (i.e. the mean vorticity direction of the steady shear flow), but the reason for the emergence of this asymmetry (at large dissipation levels) remains unclear with periodic boundary conditions along  $z$ .

Our data on high-velocity tails of  $P(C)$  and  $P(\Omega)$  have been fitted with stretched exponential functions [7] of the form  $P(x) \sim \exp(-\gamma_x x^{\alpha_x})$ , where  $\alpha_x$  and  $\gamma_x$  (with  $x = C, \Omega$ ) are the exponent

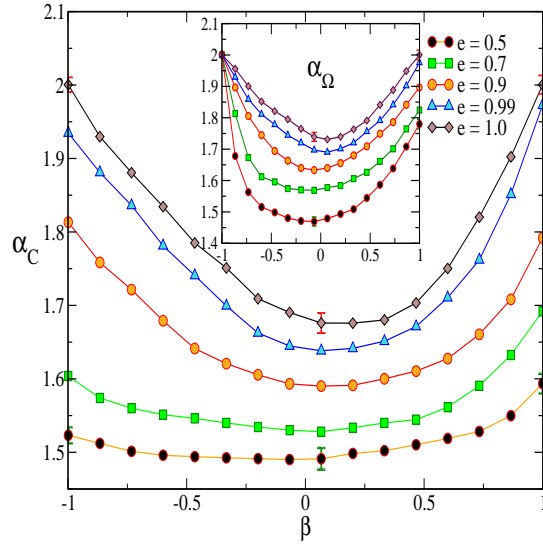


FIG. 4: (color online) Variation of the exponent for the stretched exponential,  $\alpha_i$ , with  $\beta$ ; translational (main panel,  $\alpha_C$ ) and rotational (inset,  $\alpha_\Omega$ ) velocity. Typical error-bars are shown on few data points.

and pre-factor of the corresponding distribution. Figure 4 shows the variations of  $\alpha_C$  (main panel) and  $\alpha_\Omega$  (inset) with roughness  $\beta$  for different  $e$ . For  $e = 1$  the tails of both translational and rotational VDFs deviate from a Gaussian (except at  $\beta = \pm 1$  for which  $\alpha_C = 2 = \alpha_\Omega$ ), and the functional-forms of  $\alpha_C$  and  $\alpha_\Omega$  are asymmetric and symmetric (around  $\beta = 0$ ), respectively. With increasing inelasticity, both  $\alpha_C$  and  $\alpha_\Omega$  decrease sharply, and  $\alpha_\Omega$  also becomes asymmetric around  $\beta = 0$ . A least-square fit to our data suggests that  $\alpha_i$  follows a power-law relation with inelasticity:  $\alpha_i = 2 - A_i(1 - e^2)^{B_i}$  with  $i = C, \Omega$ , and  $(A_C, B_C) \approx (5/8, 2/3)$  at  $\beta = -1$ , and  $(A_C, B_C) \approx (3/4, 1)$  and  $(A_\Omega, B_\Omega) \approx (3/8, 7/8)$  at  $\beta = 1$ . Due to the asymmetry of  $\alpha_C$  and  $\alpha_\Omega$  around  $\beta = 0$ , we could not find an universal scaling of  $\alpha_C$  and  $\alpha_\Omega$  with  $(1 - \beta^2)$  at any  $e$ .

Lastly, the variations of spatial translational velocity correlation function,  $G_{CC}^{xx}(r/d) = \langle C_x(R)C_x(R+r) \rangle$ , for different  $e$  are shown in fig. 5 for  $\beta = 0$  (main panel) and  $\beta = -0.999$  (inset)— other velocity components follow a similar behavior. It is seen that  $G_{CC}^{xx}$  (and related correlation length) increases with increasing inelasticity for a given  $\beta$ , and the effect of rotational dissipation ( $\beta$ ) is more prominent in the quasi-elastic limit ( $e \sim 1$ ). (We have checked that the pair correlation function,  $g(r/d)$ , for any  $\beta$  (not shown) is featureless, except that its contact value increases slightly with decreasing  $e$ .) A general finding is that in the quasi-elastic limit the density and spatial velocity correlations are negligible near  $\beta = \pm 1$ , however, the spatial correlations for translational velocities emerge with increasing rotational dissipation and becomes strong near

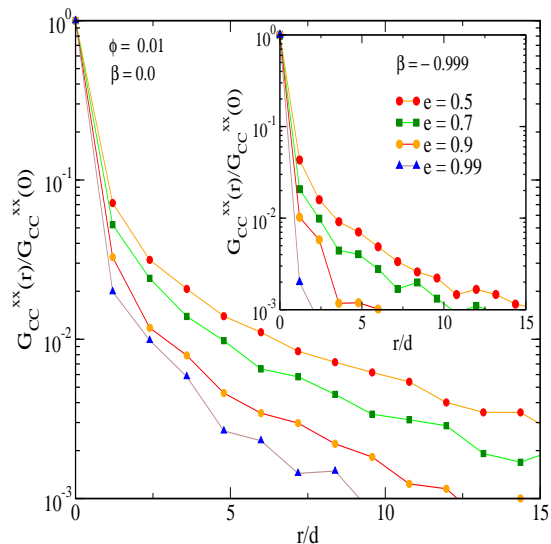


FIG. 5: (color online) Spatial velocity correlation:  $\beta = 0$  (main panel) and  $\beta = -0.999$  (inset).

$\beta = 0$ . These velocity correlations, together with orientational correlations, are responsible for non-Gaussian VDFs in a rough granular gas.

In conclusion, we showed that the translational and rotational velocities are directionally correlated in a dilute sheared granular gas, but there is no orientational correlation-induced singularity at both the perfectly smooth ( $\beta = -1$ ) and rough ( $\beta = 1$ ) limits for  $e = 1$ . Even though the translational and rotational degrees of freedom are uncorrelated at  $\beta = -1$  for any value of  $e$ , the smooth-limit ( $\beta \rightarrow -1$ ) is singular (i.e.  $\langle \Lambda \rangle \neq 0$ ) for any  $e \neq 1$ . Both ‘translational’ and ‘rotational’ VDFs remain close to a Gaussian for these two limiting cases; away from  $\beta = \pm 1$ , the orientational correlations and spatial velocity correlations are responsible for the emergence of non-Gaussian VDFs. The tails of both VDFs follow stretched exponentials, with the exponents depending on two restitution coefficients ( $e$  and  $\beta$ ). One immediate consequence of our results is the resolution of a doubt [5] that in a dilute sheared granular gas the perturbative expansions around the smooth (and also rough) limit is appropriate with Gaussian being the leading-order VDF [4].

**Acknowledgement:** We acknowledge partial funding support from the Max-Planck Society, Germany, for the ‘Max-Planck Partner Group for Topography Formation’ at JNCASR.



- [2] C. Lun, J. Fluid Mech. **233**, 539 (1991); A. Goldshtein and M. Shapiro, J. Fluid Mech. **282**, 75 (1995); M. Alam and P.R. Nott, J. Fluid Mech. **343**, 267 (1997); N. Mitarai, H. Hayakawa and H. Nakanishi, Phys. Rev. Lett. **88**, 174301 (2002); B. Gayen and M. Alam, J. Fluid Mech. **367**, 195 (2006).
- [3] M. Huthmann and A. Zippelius, Phys. Rev. E **56**, R6275 (1997); S. McNamara and S. Luding, Phys. Rev. E **58**, 2247 (1998); Herbst *et al.*, Phys. Fluids **17**, 107102 (2005).
- [4] I. Goldhirsch, S.H. Noskowitz, and O. Bar-Lev, Phys. Rev. Lett. **95**, 068002 (2005).
- [5] N.V. Brilliantov, T. Pöschel, W.T. Kranz and A. Zippelius, Phys. Rev. Lett. **98**, 128001 (2007).
- [6] S.J. Moon, J.W. Swift, and H.L. Swinney, Phys. Rev. E **69**, 011301 (2004).
- [7] S. Esipov and T. Pöschel, J. Stat. Phys. **86**, 1385 (1997); T. van Noije and M. Ernst, Gran. Matt. **1**, 52 (1998).
- [8] R. Caferio, S. Luding and H.J. Herrmann, Phys. Rev. Lett. **84**, 6014 (2000); J.S. vanZon and F.C. Mackintosh, Phys. Rev. Lett. **93**, 038001 (2004) K.C. Vijayakumar and M. Alam, Phys. Rev. E **75**, 051306 (2007).
- [9] W. Losert, D. Cooper, J. Delour, A. Kudroli, and J.P. Gollub, Chaos **9**, 682 (1999); F. Rouyer and N. Menon, Phys. Rev. Lett. **85**, 3676 (2000).
- [10] B. Lubachevsky, J. Comp. Phys. **94**, 255 (1991).
- [11] A. Lees and S. Edwards, J. Phys. C **5**, 1921 (1972); M. Alam and S. Luding, Phys. Fluids **17**, 063303 (2005).